Transparent Stretchable Self-Powered Patchable Sensor Platform with Ultrasensitive Recognition of Human Activities

Byeong-Ung Hwang,[†,⊥] Ju-Hyuck Lee,[‡,⊥] Tran Quang Trung,[†,⊥] Eun Roh,[‡] Do-Il Kim,[†] Sang-Woo Kim,[*,†,‡] and Nae-Eung Lee[*,†,‡,§]

[†]School of Advanced Materials Science & Engineering, [‡]SKKU Advanced Institute of Nano Technology (SAINT), and [§]Samsung Advanced Institute for Health Sciences & Technology (SAIHST), Sungkyunkwan University, Suwon, Kyunggi-do 16419, Republic of Korea. [⊥]B.-U.H., J.-H.L., and T.Q.T. contributed equally to this work.

ABSTRACT Monitoring of human activities can provide clinically relevant information pertaining to disease diagnostics, preventive medicine, care for patients with chronic diseases, rehabilitation, and prosthetics. The recognition of strains on human skin, induced by subtle movements of muscles in the internal organs, such as the esophagus and trachea, and the motion of joints, was demonstrated using a self-powered patchable strain sensor platform, composed on multifunctional nanocomposites of low-density silver nanowires with a conductive elastomer of poly(3,4-ethylenedioxythiophene):polystyrenesulfonate/polyurethane, with high sensitivity, stretchability, and optical transparency. The ultra-low-power consumption of the sensor, integrated with both a supercapacitor and a triboelectric nanogenerator into a single transparent stretchable platform based on the same nanocomposites, results in a self-powered monitoring system for skin strain. The capability of the sensor to recognize a wide range of strain on skin has the potential for use in new areas of invisible stretchable electronics for human monitoring. A new type of transparent, stretchable, and ultrasensitive strain sensor based on a AgNW/PEDOT:PSS/PU nanocomposite was developed. The concept of a self-powered patchable sensor system integrated with a supercapacitor and a triboelectric nanogenerator that can be used universally as an autonomous invisible sensor system was used to detect the wide range of strain on human skin.

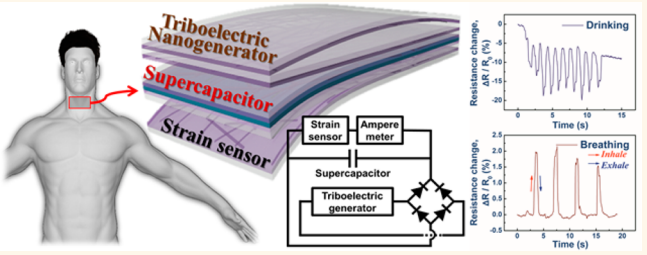

KEYWORDS: transparent and stretchable electronics · strain sensor · Ag nanowire · PEDOT:PSS · elastomer · nanocomposite · human activity

As a simple approach for monitoring human activities, body-attachable sensors can be applied to measure the strain induced on the human body by muscle movements during body motions and the functions of the internal organs. Stretchable strain sensors attached to the joint areas[1−14] or on the skin near the moving joints[15] can detect large body motions by measuring a few percent strain or larger. To detect these large strains, the required strain sensitivity does not need to be high; however, such strain sensors must have high stretchability. Conversely, to detect very small strains on the skin induced by muscle movements during the functioning of internal organs, in the range of a few tenths of a percent and lower, high strain sensitivity in a small strain range is critical. Even though internal organs have been monitored by measuring pulse rate,[16−21] respiration,[8,9,12,13] or speaking[7−9,22,23] using flexible strain sensors attached to the wrist or neck,[13,20] only a few stretchable strain sensors able to be placed in contact with human skin and capable of recording high signal quality have been investigated. For strain sensors on visible parts of the human body, such as the face or neck, that are intended for long-term use, optical transparency is preferred for aesthetic reasons. Furthermore, it is essential that the sensors in wearable smart electronics have ultra-low-power consumption to allow for prolonged operation with minimal battery exchange. Therefore, strain sensors should

* Address correspondence to kimsw1@skku.edu, nelee@skku.edu.

Received for review March 26, 2015 and accepted August 16, 2015.

Published online August 17, 2015
10.1021/acsnano.5b01835

have wide dynamic strain ranges, ultrahigh sensitivity, optical transparency, large stretchability, stability, and ultra-low-power consumption. In addition, they should demonstrate stable contact with human skin and be capable of high signal quality. Improving strain-sensing devices so that they have all of the aforementioned characteristics is a challenging task, as there is a lack of materials that can be used to fulfill the multitude of requirements.

One approach for creating strain sensors that meet the aforementioned requirements of high stretchability, ultra-low-power consumption, ultrahigh sensitivity, optical transparency, and a large dynamic range is to use elastomeric piezoresistive nanocomposites with conducting nanofillers. These fillers can be used to control electrical conductivity, strain sensitivity, and optical properties due to the fact that networked nanofillers with percolation transport between adjacent nanofillers under mechanical deformation show strong resistance modulation. Previously, stretchable nanocomposite strain sensors, such as carbon nanotubes (CNTs),[2,12,24,25] silver nanowires (AgNWs),[6] graphene nanosheets,[3,9] and metal nanoparticles,[26] were shown to produce a gauge factor (GF), ranging up to 35. The GF is defined as $(\Delta R/R_0)/\varepsilon$, where $\Delta R/R_0$ is the relative change in resistance of the strain sensor and ε is the applied strain. However, the sensitivity of such sensors at low strain has not yet been investigated, and the sensors are not often optically transparent due to the high loading of nanofillers. There is also a distinct lack of research focusing on strain sensors with ultra-low-power consumption (see Table S1 in Supporting Information).

In this research, we focused on self-powered, transparent, stretchable, ultrasensitive, and patchable strain sensors composed on multifunctional nanocomposite materials for the detection of various human activities. The devices were enabled using a multifunctional and solution-processable nanocomposite of low-density AgNWs with a conductive elastomer of poly(3,4-ethylenedioxythiophene):polystyrenesulfonate (PEDOT:PSS)/polyurethane (PU), providing high stretchability, optical transmittance, and high strain-responsive electrical properties. Conductive composite elastomers of PEDOT:PSS/PU were readily formed using environmentally benign solution processing based on water-based solutions of two components. In addition, the resistance level was controlled to facilitate ultra-low-power consumption. In this research, we tested a conformable strain sensor with a stretchability up to 100%, optical transparency with a transmittance of 75.3%, responsivity with a GF as high as 12.4 at a low strain range, and good linearity, high stability, a wide sensing range, and a power consumption as low as 5 μWcm^{-2}. The sensor device also exhibited good reproducibility after cyclic stretching at 60% of the strain. The low-power consumption allowed the strain sensors to be driven by a supercapacitor (SC), whose electrodes were made of the same nanocomposite as the one used for the strain sensor that was charged using a triboelectric nanogenerator (TENG) made of the same electrode materials. The detection of human activities (breathing, coughing, drinking, swallowing, and eating) that induce small strains and body motions that cause large strains were demonstrated using the SC charged by the TENG. We developed a novel transparent, stretchable, self-powered, all-in-one, integrated, patchable sensor platform based on a single multifunctional material system.

RESULTS AND DISCUSSION

A schematic illustration of the patchable integrated devices at various locations on human body such as neck, forearm, and fingers is shown in Figure 1a. The devices stacked into an integrated platform can be conformally attached to the joint, neck, or any other areas on which strains are induced by daily activities. The TENG can be operated by tapping by hand or joint motion. The schematics of the transparent stretchable TENG, SC, and strain sensor are illustrated in

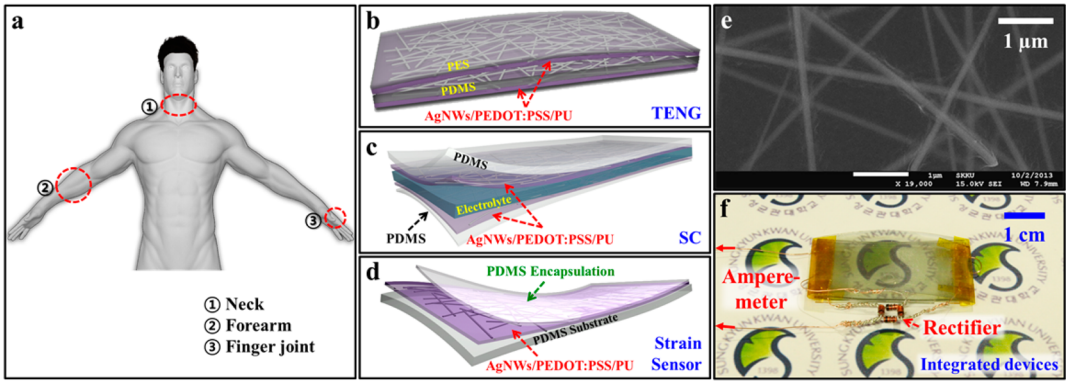

Figure 1. Schematic descriptions of the TENG, SC, and strain sensor. (a) Schematic illustration of patchable integrated devices on the neck, forearm, and finger joint. Schematic illustrations of individual components: (b) TENG, (c) SC, and (d) strain sensor. Images of the materials and integrated devices: (e) FE-SEM image of the AgNW/PEDOT:PSS/PU nanocomposite film on PDMS substrate. (f) Photograph of the vertically integrated devices of strain sensor (bottom), SC (middle), and TENG (top).

Figures 1b–d, respectively. The transparent stretchable strain sensor was formed by spin-coating a water-soluble solution of PEDOT:PSS/PU on AgNWs that are then spin-coated on oxygen plasma-pretreated polydimethylsiloxane (PDMS) substrate. The top surface is then encapsulated with another PDMS layer. The transparent and stretchable nanocomposite films of AgNWs/PEDOT:PSS/PU were used as one of the electrodes in the TENG and both of the electrodes in the SC. The TENG electrodes were formed by spin-coating the same nanocomposites of AgNWs/PEDOT:PSS/PU onto PDMS and poly(ether sulfone) (PES) substrates. A detailed fabrication process of the AgNW/PEDOT:PSS/PU nanocomposite layers of the substrates is illustrated in Figure S1a and is explained in the Experimental Section. A typical top-view field-emission scanning electron microscopy (FE-SEM) image (Figure 1e) of the AgNW/PEDOT:PSS (14%)/PU (86%) nanocomposite film shows a network of low-density AgNWs in random orientation. When water-soluble PEDOT:PSS/PU is spin-coated onto the AgNW film, the PEDOT:PSS/PU penetrates the AgNW network, due to its low viscosity and low surface energy. When the PEDOT:PSS/PU layer is cured, it links with the embedded AgNWs, resulting in three-component nanocomposites. However, the AgNWs inside the elastic conductive PEDOT:PSS/PU layer are weakly connected and slightly overlap. These features allow the AgNWs to slide over one another, producing a change in electrical conductance due to the strain induced by stretching or bending. Figure S1b shows photographs of the transparent stretchable sensor with an optical transmittance of 75.3% and a stretch of 100%. Figure 1f shows a photograph of the vertically integrated transparent devices of strain sensor, SC, and TENG.

To determine the effects of PEDOT:PSS/PU concentration ratio on the electrical and optical properties of the nanocomposites, we measured the sheet resistance and optical transmittance of the formed nanocomposite layers. For the sake of comparison, the sheet resistance values of the two-component (PEDOT:PSS/PU) and three-component (AgNW/PEDOT:PSS/PU) nanocomposite films were measured in the absence of strain (Figure 2a). The data indicate that the initial sheet resistance of the two-component film can be significantly reduced by adding AgNW nanofillers and increased by adding PU. To evaluate the optical transmittance, we measured the total optical transmission through the nanocomposite film including the PDMS substrate. As shown in Figure 2b, the optical transmittance of the nanocomposite films ranged from 71.2 to 75.3% at a wavelength of 550 nm, depending on the PEDOT:PSS/PU concentration ratio. The transmittance increased with increasing PU concentration. The inset in Figure 2b shows a photograph of a nanocomposite film on the PDMS substrate (red-dashed line), where the nanocomposite layer was sufficiently transparent

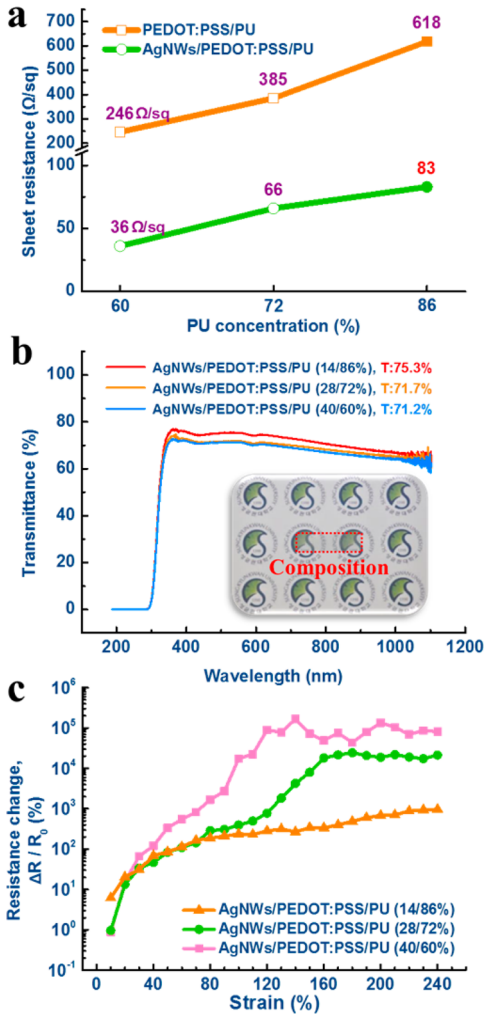

Figure 2. Characterization of nanocomposite films. (a) Sheet resistance (Ω/sq) of the PEDOT:PSS/PU film and AgNW/PEDOT:PSS/PU nanocomposite film as a function of PU concentration. (b) Transmission spectra of the AgNW/PEDOT:PSS/PU nanocomposite film with different proportions of PU. Inset: Photographs of the nanocomposite film on the PDMS substrate (red-dashed line). (c) Relative resistance change ($\Delta R/R_0$) *versus* strain of the AgNW/PEDOT:PSS/PU nanocomposite film with different PEDOT:PSS/PU concentrations.

to allow clear visualization of the logo below the strain sensor.

Next, we analyzed the use of the three-component nanocomposite as a sensing layer in a strain sensor, in addition to its use as electrodes in TENG and SC. To do this, we examined the electrical properties of the three-component nanocomposite at different concentrations of PEDOT:PSS/PU (40/60, 28/72, and 14/86%) under mechanical strain. Figure 2c shows the resistance change in the nanocomposite layers with different PEDOT:PSS/PU concentrations, which increased with increased stretching (from 10 to 240% strain). The strain response increased in a nonlinear fashion as the PU concentration decreased. Plotting the data in Figure 2c in a linear scale (see Supporting Information Figure S2a–c) clearly indicates that the resistance of the nanocomposite films with concentrations of

PEDOT:PSS/PU at 40/60 and 28/72% increases at 80 and 110% of strain, respectively, but that of the nanocomposite film with a concentration of PEDOT:PSS/PU at 14/86% is more stable with two distinct regimes at 0−130 and 130−240% (Figure S2c). The response of the nanocomposite film with a concentration of PEDOT:PSS/PU at 14/86% to low strain range (<20%) is slightly higher than that of the nanocomposite films with a concentration of PEDOT:PSS/PU at 40/60 and 28/72% (Figure S2d). The nonlinear and different changes in strain responses of the nanocomposite films with different concentrations are presumably attributed to difference in behavior of PEDOT:PSS polymer chains under large straining, even though the mechanism is not clearly understood. In addition, measurements of multiple nanocomposite samples with the same PEDOT:PSS/PU concentration at 14/86% under applied strain of 0−240% show similar trends in electrical responses (Figure S2e). Considering high-performance strain sensors and electrodes with high stability and stretchability for TENG and SC, we chose the AgNW/PEDOT:PSS/PU (14/86%) nanocomposite for device fabrication.

The electrical and optical properties of strain sensors with different density of AgNWs are shown in Figure S3. The device with a high density of AgNWs (spin-coating condition of 200 rpm) showed higher responsivity in comparison with that of the devices with a medium and low density of AgNWs (spin-coating condition of 250 and 300 rpm, respectively) (Figure S3a). However, the optical transmittance decreased at higher density of AgNWs (Figure S3b). In addition, the power consumption increased with higher density of AgNWs. For performance optimization of a self-powered transparent sensor platform, therefore, three parameters of responsivity, transparency, and power consumption need to be compromised. In the experiment, the medium density of AgNWs for fabrication of strain sensors was chosen.

To demonstrate the advantages of the three-component nanocomposite compared to those of the two-component (PEDOT:PSS/PU) composite for strain sensing, we examined the hysteresis, responsivity, and stability of each of the devices under mechanical deformation. Figure S4 shows the resistance variation of the two-component and three-component composites during cyclic stretching−releasing tests (10 000 cycles) at a tensile strain of 40%. The baseline drift in the resistance in the two-component composite (S4a) was higher than that in the three-component nanocomposite (Figure S4b). The results demonstrate that the three-component nanocomposite strain sensor showed high responsivity, high stability, and low hysteresis in comparison with the two-component composite strain sensor. For a better understanding of the hysteresis and stability of the two-component and three-component composites, the surfaces of these films were analyzed using FE-SEM and atomic force microscopy (AFM), the results of which are shown in Figure S5. Some cracks were revealed in the three-component nanocomposite film after being cyclically stretched 10 000 times at a 40% strain; these cracks were believed to be the cause of the observed baseline drift. The FE-SEM and AFM images of the PEDOT:PSS/PU film shown in Figure S5a,c demonstrated much more severe cracking than did the AgNW/PEDOT:PSS/PU film shown in Figure S5b,d.

The physical phenomenon responsible for the electromechanical differences between the two-component and three-component composites can be explained by the interactions between PEDOT:PSS and PU and between the AgNWs and PEDOT:PSS/PU composites. In the two-component composite, the weak interactions between PU and PEDOT:PSS suggest that the PEDOT:PSS polymer chains slip or break, as shown in Figure S5a,c, and do not recover or re-form, respectively, during the unloading cycle.[27] This leads to high hysteresis, low responsivity, and poor stability. Because of the much higher Young's modulus of AgNWs[28,29] compared to that of the PEDOT:PSS/PU composite, the AgNWs in the three-component nanocomposite can be regarded as rigid elements during the stretch/release cycles, which help to reduce cracking, as shown in Figure S5b,d. Interactions of rigid AgNWs and polymer chains inside the matrix can possibly reduce the crack propagation by pinning, bridging, or deflecting cracks.[30] Moreover, the sensing mechanism of the three-component nanocomposites was mainly attributed to percolation transport between adjacent AgNWs, resulting in strong modulation in the resistance of networked AgNWs under mechanical deformation. In the longitudinal direction of stretch/release, the gaps between the ends of the AgNWs increased/decreased, leading to a decrease/increase in the number of electrical pathways. Subsequently, the electrical resistance of the networked AgNWs increased/decreased. These features lead to high responsivity, good stability, and low hysteresis in three-component nanocomposite devices.

To further investigate the strain-sensing performance of the nanocomposite sensor, we studied the sensing characteristics during repetitive straining conditions by measuring the time-dependent changes in the normalized resistance ($\Delta R/R_0$) under various strains. The sensors were strained using two different mechanical modes: a bending mode for low tensile and compressive strains and a stretching mode for high tensile strain. Figure 3 shows the typical responses and GFs of the strain sensor based on the AgNW/PEDOT:PSS/PU (14/86%) nanocomposite according to the systematic straining tests. Figure 3a,c shows the $\Delta R/R_0$ *versus* time curves under low strain tests (1.5−6%) in the tensile and compressive cyclic bending modes (50 cycles per pulse), respectively. The GF values under low tensile and compressive strains, extracted from Figure 3a,c, respectively, are presented

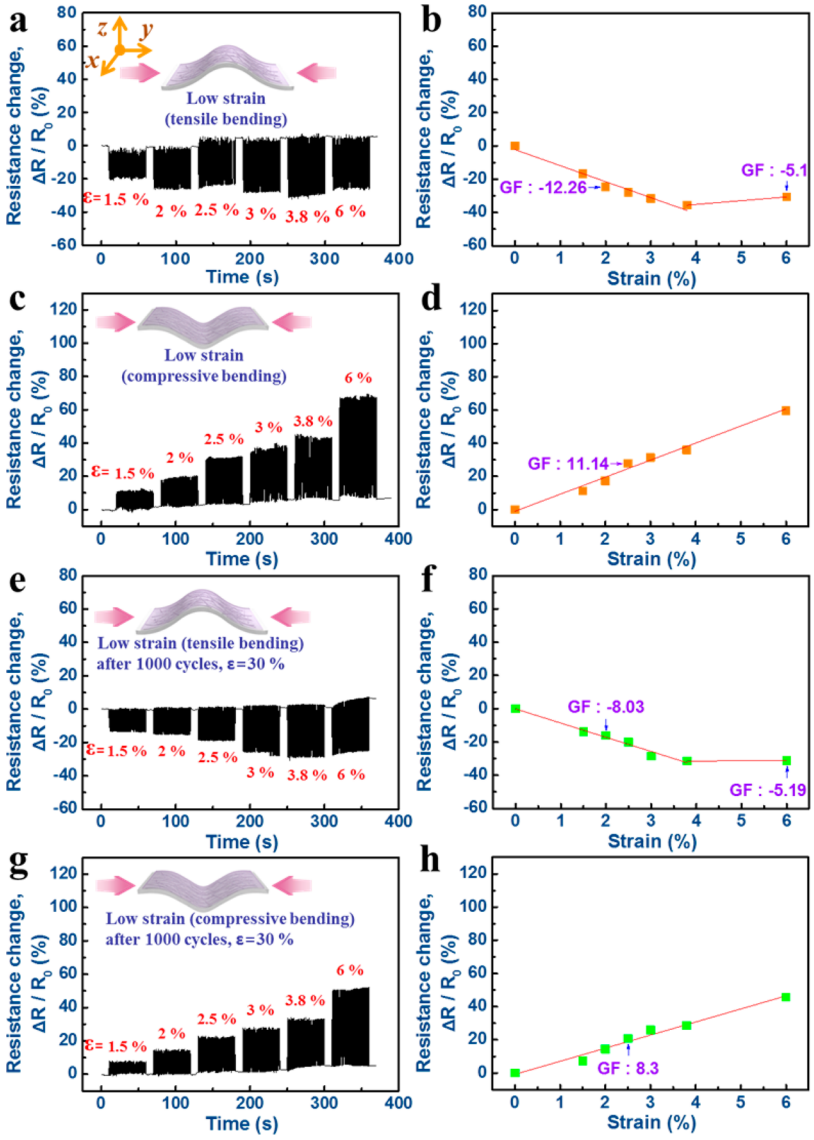

Figure 3. Systematic straining tests of the AgNW/PEDOT:PSS/PU (14/86%) nanocomposite resistive strain sensors. (a,c,e,g) Resistance change ($\Delta R/R_0$) of the nanocomposite strain sensor *versus* time under progressively increasing strain from 1.5 to 6% (low strain) in tensile and compressive cyclic bending modes with 50 cycles per pulse before (a,c) and after (e,g) 1000 cycles of stretching. (b,d,f,h) Resistance change ($\Delta R/R_0$) *versus* low strain under tensile and compressive bending before (b,d) and after (f,h) 1000 cycles of stretching.

in Figures 3b,d. The $\Delta R/R_0$ decreased under the low tensile strain and increased under the low compressive strain, which enabled us to discern the contractional and expansional movements of the skin. The opposite $\Delta R/R_0$ variation under tensile and compressive strain is caused by the multistage stacking of the AgNW network, where the number of electrical interconnections or current paths can be modulated under mechanical deformation. Under the bending mode, the three-component film can be deformed in the *y*-direction (in-plane direction) and the *z*-direction (out-of-plane direction). However, at low strain (large bending radius), the deformation in the *z*-direction is more dominant than that in the *y*-direction. Therefore, tensile strain may reduce the thickness of the three-component film, leading to a decrease in the contact resistance (R_c) between the networked AgNWs and, thus, a decrease in the resistance of the nanocomposite. These results are illustrated in Figure 3a,b. Conversely, the resistance increased as the compressive strain increased, as shown in Figure 3c,d, as a result of the decrease in R_c between the AgNWs, presumably due to an increase in the thickness of the three-component nanocomposite.

In order to evaluate the reliability of the sensor device after repetitive mechanical deformations, we examined the responsivity, repeatability, response time, and relaxation time after cyclic stretching. Figure 3e,g shows the resistance response curves *versus* time from the low strain tests (1.5−6%) in tensile and compressive cyclic bending modes after 1000 stretching cycles at a strain of 30%. The repeatability, response time, and relaxation time of the device after cyclic stretching were nearly

unchanged. However, the GF of the device decreased from 12 to 8 in tensile bending mode and from 11 to 8 in compressive bending mode after cyclic stretching (Figure 3f,h). This phenomenon is, in part, due to the interaction between the AgNW filler and the PEDOT:PSS/PU composite matrix. After cyclic stretching, the deformation of the three-component nanocomposite increases the friction force between the AgNWs and the PEDOT:PSS/PU matrix so that the AgNWs buckle above a certain threshold frictional force. As a result, the AgNWs cannot return to their initial positions. This increases the gaps between the ends of the AgNWs, leading to a reduction in the continuity of the AgNW network and subsequently decreasing the number of electrical pathways.[6] The decreased pathway number leads to a decrease in the responsivity or GF of the sensing layer of the device.

To demonstrate that the sensor device can function under high strain levels, we analyzed the responsivity of the device to strain ranging from 10 to 60%. Supporting Information Figure S6a shows resistance response *versus* time curves under high tensile strain in stretching mode. The resistance change *versus* strain with GF is shown in Figure S6b, which indicates that the resistance continued to increase under high tensile strain. During stretching, the gaps between the ends of the AgNWs increased, resulting in a decrease in the number of electrical pathways; therefore, the electrical resistance of the three-component nanocomposite increased. We also examined the responsivity and repeatability of the device after cyclic stretching. Figure S6c,d presents the resistance change under strain ranging from 10 to 60% and the GF of the nanocomposite sensor after 500 cycles of stretching. Neither the strain responsivity nor GF of the sensor was significantly changed after cyclic stretching. Furthermore, the GF of the sensor at high strain was slightly greater than 1, thus demonstrating the stability of our strain sensor.

To compare the sensing responses of the three-component and two-component composites, we fabricated two types of two-component composite strain sensors (PEDOT:PSS/PU (14/86%) and AgNW/PU). Figure S7 shows typical responses and GF values of the two-component composite strain sensors. The PEDOT:PSS/PU strain sensor presented low responsivities at both low strain (GF = 2.6−2.9) and high strain (GF = 1.07), as shown in Figure S7a−c. The AgNW/PU strain sensor also showed low responsivity and instability at high strain, as demonstrated in Figure S7d. These results demonstrate that strain sensors based on three-component nanocomposites are more advantageous than those based on two-component composites.

In order to determine the capabilities of our highly transparent, stretchable, and sensitive nanocomposite strain sensor for monitoring human activities by detecting strains caused by muscle motions, the sensor was attached to the neck of a healthy subject in an attempt to noninvasively monitor the muscle movements of the trachea (breathing and coughing) and esophagus (drinking, swallowing, and eating) (Figure 4a). As shown in Figure 4b−f, the strain sensor exhibited high sensitivity and distinct patterns, allowing us to differentiate between the signals generated by the trachea and esophagus when breathing, coughing, drinking water, swallowing saliva, and eating. There were, in particular, significant differences between the signals generated during saliva swallowing *versus* the gathering of saliva, as shown in Figure 4e.

In addition, to monitor the strain modulation on human skin caused by muscle movement, we attached the device to one subject's forearm (Figure S8a). This allowed us to detect and distinguish muscle movements for different motions. The device was able to easily detect and discriminate various human motions. Different signal patterns were generated for instances where the subject repeatedly clenched a fist, with holding times of 2 and 0.5 s, respectively (Figure S8b,c) or moved the wrist up and down (Figure S8d) or in a circle (Figure S8e).

To further investigate the responsivity of the strain sensor to large-scale human motions, strain sensors were placed on the index finger of a subject. The highly stretchable sensor showed a good responsivity to the movements of the index finger (Figure S8f).

The results in Figure 4 and Figure S8 indicate the high sensitivity and good repeatability of devices to strain variation caused by muscle movements. The sensor was able to distinguish between the various motions, showing distinct signal patterns for each of the motions. These results show that skin strain monitoring is an effective method for monitoring body motions and the functions of internal organs. Our results showed that the sensor accurately measured the deformation of the epidermis and muscles around the throat during breathing, coughing, drinking, swallowing, and eating, as well as various movements of index finger. Future applications might expand to include sophisticated activity recognition in biomedical fields and remote control of human−machine interfaces.

To demonstrate that the strain sensor can be operated using a power source of the SC that is charged by the TENG, we developed a transparent and stretchable SC and TENG (Figure 4g) and analyzed their performances (Figures S9−S12). The performance of the TENG was determined as a function of load resistance, and the maximum output peak power was observed at a load resistance of 50 MΩ (Figure S9). The performance of the SC was characterized using a capacitance−voltage (*C*−*V*) curve and a charge−discharge curve at different scan rates and current densities, respectively. The areal capacitance of the SC was 190 μF/cm^2 at a

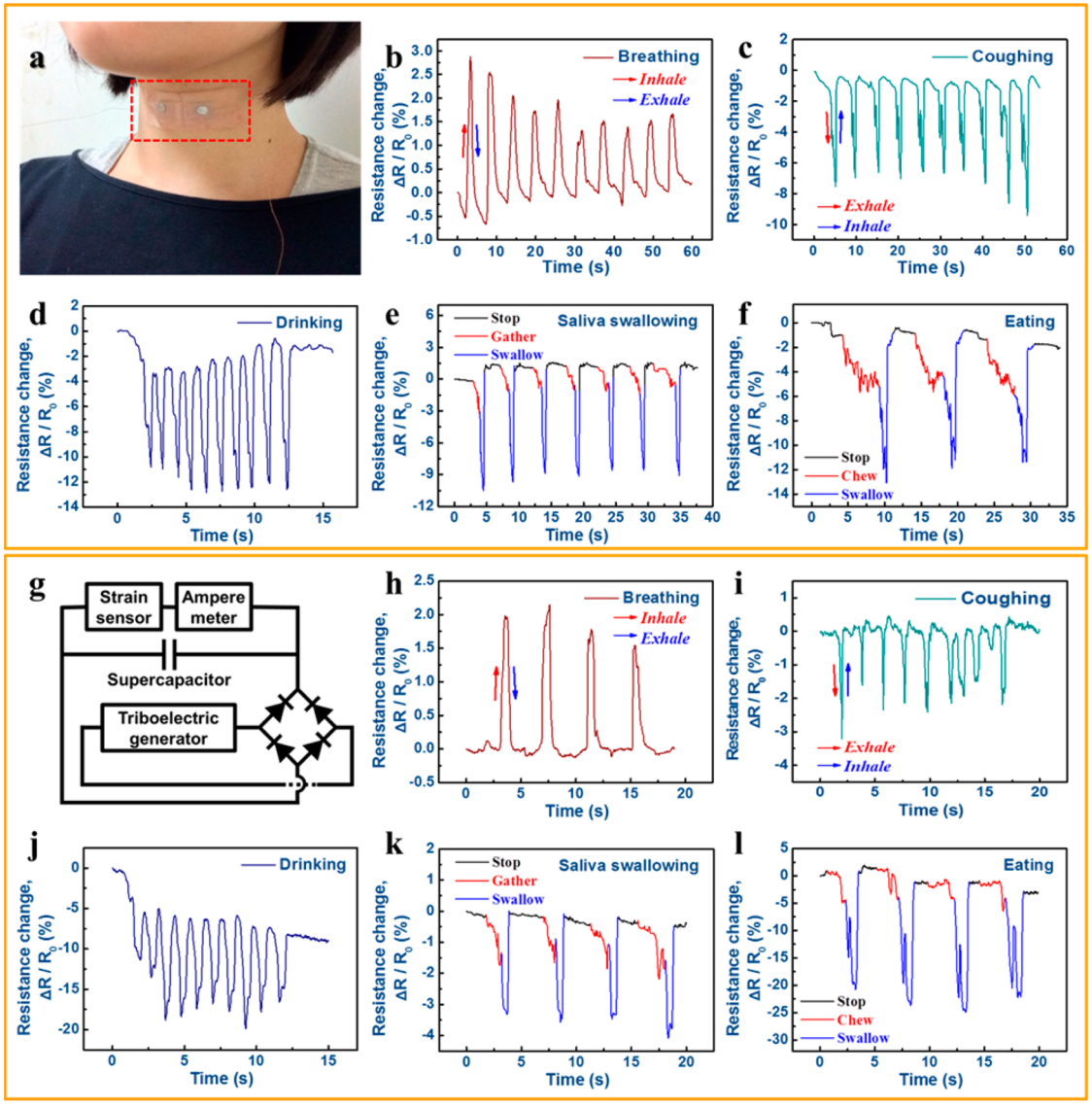

Figure 4. Monitoring of strain caused by muscle movement for functions of the trachea and esophagus. (a) Stretchable and transparent strain sensor attached to the neck. (b–f) Resistance change ($\Delta R/R_0$) of the nanocomposite strain sensor *versus* time, measured by a source measurement unit, during breathing, coughing, drinking, saliva swallowing, and eating, respectively. (g) Circuit diagram of strain according to the sensor with SC charged by TENG. (h–l) Resistance change ($\Delta R/R_0$) of the nanocomposite strain sensor *versus* time, measured by SC charged by TENG, during breathing, coughing, drinking, saliva swallowing, and eating, respectively.

scan rate of 50 mV/s and a current density of 369 μF/cm^2 at 4 μA/cm^2 (Figure S10). The stretchability of the SC was confirmed by measuring the $C-V$ curve before and after 5000 cycles of stretching at 30% strain (Figure S11). The charging property of the SC determined using the rectified output from the TENG is presented in Figure S12. Figure 4h–l shows modulation of the strain sensor for the various muscle movements of the human esophagus (drinking and swallowing) and trachea (breathing and coughing), which were measured using the SC charged by the TENG. The strain sensor showed high responsivity, and the sensor responses had the same patterns and tendencies as when using an external power source (Figure 4b–f). Electrical performances of the integrated devices measured under mechanical stretching are shown in Figure S13. The integrated device platform was stretched to 10% of strain, and then cyclic pushing was applied on the TENG to generate the power (Figure S13a) and store the generated power into SC (Figure S13b). Then, we used the stored power to measure the responsivity of the strain sensor to cyclic straining (Figure S13c). These results demonstrate that our integrated devices also work well under the condition of mechanical stretching.

In general, our results indicate the multifunctionality of three-component nanocomposites of AgNW/PEDOT:PSS/PU as a self-powered, patchable strain sensor system. The composites of nonconductive elastomeric matrix and high-density AgNWs lead to high-power consumption, large hysteresis, low responsivity and

stability, and no optical transparency due to the decreased tunability of the electrical and optical properties. Furthermore, a two-component conductive elastomeric composite of the nonconductive elastomer and conductive polymer resulted in low sensitivity to strain due to a lack of change in the percolating charge transport of the composite under straining; therefore, it is necessary to consider a new approach for strain-sensing materials based on low-density AgNWs embedded in an elastomeric conductive polymer matrix with the goal of high sensitivity, low-power consumption, high stretchability, and high optical transparency. The three-component nanocomposites demonstrated increased networking of AgNWs and the PEDOT:PSS phase. The greater responses to the various strains can be attributed to the larger changes in percolating carrier transport due to the additional modulation of the AgNW-PEDOT:PSS junction contact resistance. Our results clearly indicate that combining low-density AgNWs and the conductive elastomer of PEDOT:PSS/PU composite resulted in tunability of electrical conductivity, sensitivity, and optical transmittance that can be used as a three-component nanocomposite sensor system.

The sensing mechanism of the strain sensor based on a three-component nanocomposite relies on the change in contact resistance between AgNWs and AgNW-PEDOT:PSS junctions under mechanical deformation. Under bending mode, the deformation of the three-component nanocomposite in the out-of plane direction was larger than that in the in-plane direction. The opposite was true for the stretching mode characteristics. The device outlined in this research is capable of effectively measuring both small and large strains. Based upon the different electrical modulations for the various straining modes, the sensor was able to distinguish between tensile and compressive strains induced on the skin by muscle movements. In addition, we devised stretchable nanocomposite devices with the addition of a very simple, low-cost fabrication process and biocompatible components (PDMS, PEDOT:PSS, and PU) that can be used to develop human monitoring devices with realistic functions.

The majority of the current stretchable strain sensors rely on external power sources, which often limits their use in practical applications in wearable electronics. Furthermore, the characteristics of power consumption in strain sensors have not been fully explored. Since body-attachable sensors should be integrated into wireless environments, such as the Internet of Everything (IoE), low-power consumption and autonomous self-powered sensing systems integrated with energy harvesting and storage functions are essential for autonomous monitoring of human activities. Therefore, there is a pressing need for the development of an integrated sensor system with power generation and storage devices that can be readily incorporated into either a wearable or body-attachable platform. Recently, there have been reports on self-powered sensor systems integrated with sensors, energy harvesters, and charge storage devices.[31−35] In these approaches, a variety of materials were used for the different components of the integrated systems. Our self-powered, all-in-one, integrated sensor system, developed using multifunctional materials to show strain responsivity, intrinsic stretchability, optical transparency, and electrochemical activity, demonstrates the potential for such systems. Such a single, multifunctional material to be used for strain sensing, power generation, and storage is highly advantageous, as demonstrated in this research.

CONCLUSION

In summary, we developed a new kind of transparent, stretchable, highly sensitive, solution-processable, low-power strain sensor based on the multifunctional AgNW/PEDOT:PSS/PU nanocomposite, which can also be used for electrodes in TENG and SC in all-in-one, self-powered integrated systems. Systematic and elaborate strain tests for sensor and energy devices based on the developed multifunctional nanocomposite showed high performance, good stability, and reliability. Our study suggests that integrated sensor systems can be easily extended for integration into other sensors, such as physical, chemical, or biological sensors, and can act as a new class of patchable systems. They can, therefore, be used universally as autonomous invisible conformal sensor systems capable of subsequent integration with other components, such as signal processing and data transmission. We expect that the integrated transparent and stretchable electronic strain sensor system, with its ability to conform to deformable and arbitrarily shaped objects, can be used in a variety of applications in a multitude of fields, including personal health monitoring, soft robotics, artificial skins, and human-friendly human−machine interfaces.

EXPERIMENTAL SECTION

Materials. AgNWs dispersed in isopropyl alcohol (IPA) were purchased from Sigma-Aldrich. The mean length and diameter of the supplied AgNWs were 30 μm and 100 nm, respectively. The AgNWs were well-dispersed by the polar groups without a surfactant coating of polyvinylpyrrolidone. In order to minimize the agglomeration of nanowires and deposit them uniformly onto elastic substrates, the dispersion was diluted to a concentration of 0.5 wt % in IPA. A PDMS elastomer kit (Sylgard 184 from Dow Corning), PEDOT:PSS solution (1−1.3 wt %, CLEVIOS PH1000 from Heraues), PU (39−41 wt % Alberdingk U3251, Alberdingk Boley), DMSO, Zonyl FS-300 (Sigma-Aldrich), and Au−Ni woven conductive textile (Solueta Co. Ltd., silverized nylon/spandex knit SMP 130) were all used as purchased.

Preparation of a Conductive Elastomer Solution Blend. We chose polyurethane dispersions (PUDs) (Alberdingk U3251) for higher stretchability and uniform coating due to their dispersion of sub-micrometer-sized PU particles in water. Before blending the polymer solution, the PUD was diluted with deionized water to 4 wt %, and the PEDOT:PSS was premixed with 5−8 wt % DMSO and 1 wt % Zonyl.

During blending, the diluted PUD was stirred at a speed greater than 400 rpm while PEDOT:PSS (14, 27, or 40 wt %, premixed with DMSO and Zonyl) was added using a syringe pump. Polymer blends were filtered through a 0.45 μm syringe filter before use.

Fabrication, Characterization, and Demonstration of Strain Sensors. The transparent and stretchable strain sensor was fabricated using the following procedure. The AgNW suspension was spin-coated onto a PDMS substrate. The AgNWs were then dried to form a uniform and conductive film. Next, the PEDOT:PSS/PU nanocomposite solution was spin-coated onto the AgNW filler to prepare a three-component incorporation. Then, the nanocomponent conductive film was dried on a hot plate at 150 °C for 1 h. To minimize the ambient effects from the air atmosphere during the stretching test, the fabricated devices were encapsulated with a PDMS layer and dried on a hot plate at 120 °C for 1 h. To measure the resistance of the AgNW/PEDOT:PSS/PU nanocomposite strain sensor during the repetitive mechanical deformation caused by stretching and bending, the Au textiles as electrodes were used between the electrical contact tips and the film surface. Copper wires were subsequently attached to the two ends of the nanocomposite thin film using a silver paste, and the film was attached to various parts of the human body, including the neck, arm, wrist, and index finger using double-sided adhesive tape. To measure the stand-alone strain sensor on the human body, a source measurement unit (HP 4145B) was used. To monitor the signal modulation in the strain sensor integrated with TENG and SC, a low-noise current preamplifier (SR570, Stanford Research Systems, Inc.) was used to measure the current change during various human activities.

Preparation of TENG and SC. The TENG was fabricated using the following procedure: AgNW/PEDOT:PSS/PU nanocomposite-coated PDMS and AgNW/PEDOT:PSS/PU nanocomposite-coated PES were used for the TENG. An arch-shaped nanocomposite-coated PES was positioned on the top of the TENG. The PES surface and the side of the nanocomposite on the PDMS were placed into contact and then separated to generate electricity. A digital phosphor oscilloscope (DPO 3052, Tektronix) and a low-noise current preamplifier were used to measure the output voltage and current for characterization of the TENG while compressing the unit with 1 kgf force.

The SC was fabricated using two AgNW/PEDOT:PSS/PU nanocomposite-coated PDMS layers as electrodes for SC. To prepare the gel electrolyte, 10 g of PVA (molecular weight 89 000−98 000, 99% hydrolyzed, Aldrich) was diluted in 100 mL of DI water, and 10 g of concentrated H_3PO_4 was then added. This solution was stirred for 3 h at 90 °C to obtain a clear solution. The solution was cooled to room temperature, poured onto the clean surface of a PTFE film, and left to dry overnight. The resulting film was easily peeled off of the PTFE film surface. The PVA/H_3PO_4 film was sandwiched between the electrodes. The capacitive performance of the fabricated SC was characterized using a capacitance−voltage ($C-V$) measurement system (Biologic VMP3, France). Fabricated strain sensor, SC, and TENG devices were vertically stacked by attaching the PDMS substrates after oxygen plasma treatments. For demonstration of the strain sensor integrated with the TENG and SC, the SC was charged by the TENG by tapping.

Conflict of Interest: The authors declare no competing financial interest.

Acknowledgment. This research was supported by the Basic Science Research Program (2013R1A2A1A01015232) through the National Research Foundation (NRF), funded by the Ministry of Science, ICT & Future Planning. B.-U.H., J.-H.L., T.Q.T., S.-W.K., and N.-E.L. designed the methodology. B.-U.H., J.-H.L., and E.R. performed the experiments. S.-W.K. and N.-E.L. supervised the project. B.-U.H., J.-H.L., T.Q.T., S.-W.K., and N.-E.L. wrote the manuscript.

Supporting Information Available: The Supporting Information is available free of charge on the ACS Publications website at DOI: 10.1021/acsnano.5b01835.

Additional experimental details, figures, and table (PDF)

REFERENCES AND NOTES

1. Kim, D. H.; Lu, N.; Ma, R.; Kim, Y. S.; Kim, R. H.; Wang, S.; Wu, J.; Won, S. M.; Tao, H.; Islam, A.; et al. Epidermal Electronics. *Science* **2011**, *333*, 838–843.
2. Jung, S.; Kim, J. H.; Kim, J.; Choi, S.; Lee, J.; Park, I.; Hyeon, T.; Kim, D. H. Reverse-Micelle-Induced Porous Pressure-Sensitive Rubber for Wearable Human-Machine Interfaces. *Adv. Mater.* **2014**, *26*, 4825–4830.
3. Yan, C.; Wang, J.; Kang, W.; Cui, M.; Wang, X.; Foo, C. Y.; Chee, K. J.; Lee, P. S. Highly Stretchable Piezoresistive Graphene−Nanocellulose Nanopaper for Strain Sensors. *Adv. Mater.* **2014**, *26*, 2022–2027.
4. Muth, J. T.; Vogt, D. M.; Truby, R. L.; Mengüç, Y.; Kolesky, D. B.; Wood, R. J.; Lewis, J. A. Embedded 3D Printing of Strain Sensors within Highly Stretchable Elastomers. *Adv. Mater.* **2014**, *26*, 6307–6312.
5. Trung, T. Q.; Tien, N. T.; Kim, D.; Jang, M.; Yoon, O. J.; Lee, N.-E. A Flexible Reduced Graphene Oxide Field-Effect Transistor for Ultrasensitive Strain Sensing. *Adv. Funct. Mater.* **2014**, *24*, 117–124.
6. Amjadi, M.; Pichitpajongkit, A.; Lee, S.; Ryu, S.; Park, I. Highly Stretchable and Sensitive Strain Sensor Based on Silver Nanowire-Elastomer Nanocomposite. *ACS Nano* **2014**, *8*, 5154–5163.
7. Wang, X.; Gu, Y.; Xiong, Z.; Cui, Z.; Zhang, T. Silk-Molded Flexible, Ultrasensitive, and Highly Stable Electronic Skin for Monitoring Human Physiological Signals. *Adv. Mater.* **2014**, *26*, 1336–1342.
8. Park, J.; Lee, Y.; Hong, J.; Ha, M.; Jung, Y.-D.; Lim, H.; Kim, S. Y.; Ko, H. Giant Tunneling Piezoresistance of Composite Elastomers with Interlocked Microdome Arrays for Ultrasensitive and Multimodal Electronic Skins. *ACS Nano* **2014**, *8*, 4689–4697.
9. Boland, C. S.; Khan, U.; Backes, C.; O'Neill, A.; McCauley, J.; Duane, S.; Shanker, R.; Liu, Y.; Jurewicz, I.; Dalton, A. B.; et al. Sensitive, High-Strain, High-Rate Bodily Motion Sensors Based on Graphene-Rubber Composites. *ACS Nano* **2014**, *8*, 8819–8830.
10. Cai, L.; Song, L.; Luan, P.; Zhang, Q.; Zhang, N.; Gao, Q.; Zhao, D.; Zhang, X.; Tu, M.; Yang, F.; et al. Super-stretchable, Transparent Carbon Nanotube-Based Capacitive Strain Sensors for Human Motion Detection. *Sci. Rep.* **2013**, *3*, 3048.
11. Yao, S.; Zhu, Y. Wearable Multifunctional Sensors Using Printed Stretchable Conductors Made of Silver Nanowires. *Nanoscale* **2014**, *6*, 2345–2352.
12. Yamada, T.; Hayamizu, Y.; Yamamoto, Y.; Yomogida, Y.; Izadi-Najafabadi, A.; Futaba, D. N.; Hata, K. A Stretchable Carbon Nanotube Strain Sensor for Human-Motion Detection. *Nat. Nanotechnol.* **2011**, *6*, 296–301.
13. Wang, Y.; Wang, L.; Yang, T.; Li, X.; Zang, X.; Zhu, M.; Wang, K.; Wu, D.; Zhu, H. Wearable and Highly Sensitive Graphene Strain Sensors for Human Motion Monitoring. *Adv. Funct. Mater.* **2014**, *24*, 4666–4670.
14. Park, J.; Lee, Y.; Hong, J.; Lee, Y.; Ha, M.; Jung, Y.; Lim, H.; Kim, S. Y.; Ko, H. Tactile-Direction-Sensitive and Stretchable Electronic Skins Based on Human-Skin-Inspired Interlocked Microstructures. *ACS Nano* **2014**, *8*, 12020–12029.
15. Kim, J.; Lee, M.; Shim, H. J.; Ghaffari, R.; Cho, H. R.; Son, D.; Jung, Y. H.; Soh, M.; Choi, C.; Jung, S. Stretchable Silicon Nanoribbon Electronics for Skin Prosthesis. *Nat. Commun.* **2014**, *5*, 5747.
16. Huang, X.; Liu, Y.; Cheng, H.; Shin, W. J.; Fan, J. A.; Liu, Z.; Lu, C. J.; Kong, G. W.; Chen, K.; Patnaik, D.; et al. Materials and Designs for Wireless Epidermal Sensors of Hydration and Strain. *Adv. Funct. Mater.* **2014**, *24*, 3846–3854.
17. Pang, C.; Koo, J. H.; Nguyen, A.; Caves, J. M.; Kim, M. G.; Chortos, A.; Kim, K.; Wang, P. J.; Tok, J. B. H.; Bao, Z.

Highly Skin-Conformal Microhairy Sensor for Pulse Signal Amplification. *Adv. Mater.* **2015**, *27*, 634–640.
18. Schwartz, G.; Tee, B. C. K.; Mei, J.; Appleton, A. L.; Kim, D. H.; Wang, H.; Bao, Z. Flexible Polymer Transistors with High Pressure Sensitivity for Application in Electronic Skin and Health Monitoring. *Nat. Commun.* **2013**, *4*, 1859.
19. Gong, S.; Schwalb, W.; Wang, Y.; Chen, Y.; Tang, Y.; Si, J.; Shirinzadeh, B.; Cheng, W. A Wearable and Highly Sensitive Pressure Sensor with Ultrathin Gold Nanowires. *Nat. Commun.* **2014**, DOI: 10.1038/ncomms4132.
20. Pang, C.; Lee, G. Y.; Kim, T. I.; Kim, S. M.; Kim, H. N.; Ahn, S. H.; Suh, K. Y. A Flexible and Highly Sensitive Strain-Gauge Sensor Using Reversible Interlocking of Nanofibres. *Nat. Mater.* **2012**, *11*, 795–801.
21. Choong, C. L.; Shim, M. B.; Lee, B. S.; Jeon, S.; Ko, D. S.; Kang, T. H.; Bae, J.; Lee, S. H.; Byun, K. E.; Im, J.; et al. Highly Stretchable Resistive Pressure Sensors Using a Conductive Elastomeric Composite on a Micropyramid Array. *Adv. Mater.* **2014**, *26*, 3451–3458.
22. Kang, D.; Pikhitsa, P. V.; Choi, Y. W.; Lee, C.; Shin, S. S.; Piao, L.; Park, B.; Suh, K. Y.; Kim, T. I.; Choi, M. Ultrasensitive Mechanical Crack-Based Sensor Inspired by the Spider Sensory System. *Nature* **2014**, *516*, 222–226.
23. Yang, J.; Chen, J.; Su, Y.; Jing, Q.; Li, Z.; Yi, F.; Wen, X.; Wang, Z.; Wang, Z. L. Eardrum-Inspired Active Sensors for Self-Powered Cardiovascular System Characterization and Throat-Attached Anti-Interference Voice Recognition. *Adv. Mater.* **2015**, *27*, 1316–1326.
24. Lipomi, D. J.; Vosgueritchian, M.; Tee, B. C. K.; Hellstrom, S. L.; Lee, J. A.; Fox, C. H.; Bao, Z. Skin-Like Pressure and Strain Sensors Based on Transparent Elastic Films of Carbon Nanotubes. *Nat. Nanotechnol.* **2011**, *6*, 788–792.
25. Wang, X.; Li, T.; Adams, J.; Yang, J. Transparent, Stretchable, Carbon-Nanotube-Inlaid Conductors Enabled by Standard Replication Technology for Capacitive Pressure, Strain and Touch Sensors. *J. Mater. Chem. A* **2013**, *1*, 3580–3586.
26. Lee, J.; Kim, S.; Lee, J.; Yang, D.; Park, B. C.; Ryu, S.; Park, I. A Stretchable Strain Sensor Based on a Metal Nanoparticle Thin Film for Human Motion Detection. *Nanoscale* **2014**, *6*, 11932–11939.
27. Seyedin, M. Z.; Razal, J. M.; Innis, P. C.; Wallace, G. G. Strain-Responsive Polyurethane/PEDOT:PSS Elastomeric Composite Fibers with High Electrical Conductivity. *Adv. Funct. Mater.* **2014**, *24*, 2957–2966.
28. Keshoju, K.; Sun, L. Mechanical Characterization of Magnetic Nanowire-Polydimethylsiloxane Composites. *J. Appl. Phys.* **2009**, *105*, 023515.
29. Wu, B.; Heidelberg, A.; Boland, J. J.; Sader, J. E.; Sun, X.; Li, Y. Microstructure-Hardened Silver Nanowires. *Nano Lett.* **2006**, *6*, 468–472.
30. Srivastava, I.; Koratkar, N. Fatigue and Fracture Toughness of Epoxy Nanocomposites. *JOM* **2010**, *62*, 50–57.
31. Wang, Z. L. Self-Powered Nanosensors and Nanosystems. *Adv. Mater.* **2012**, *24*, 280–285.
32. Zhang, H.; Yang, Y.; Hou, T. C.; Su, Y.; Hu, C.; Wang, Z. L. Triboelectric Nanogenerator Built Inside Clothes for Self-Powered Glucose Biosensors. *Nano Energy* **2013**, *2*, 1019–1024.
33. Yuan, L.; Xiao, X.; Ding, T.; Zhong, J.; Zhang, X.; Shen, Y.; Hu, B.; Huang, Y.; Zhou, J.; Wang, Z. L. Paper-Based Supercapacitors for Self-Powered Nanosystems. *Angew. Chem., Int. Ed.* **2012**, *51*, 4934–4938.
34. Yang, Y.; Zhang, H.; Chen, J.; Lee, S.; Hou, T. C.; Wang, Z. L. Simultaneously Harvesting Mechanical and Chemical Energies by a Hybrid Cell for Self-Powered Biosensors and Personal Electronics. *Energy Environ. Sci.* **2013**, *6*, 1744–1749.
35. Jung, S.; Lee, J.; Hyeon, T.; Lee, M.; Kim, D. H. Fabric-Based Integrated Energy Devices for Wearable Activity Monitors. *Adv. Mater.* **2014**, *26*, 6329–6334.